THE ASTROPHYSICAL JOURNAL, 525:759–771, 1999 November 10

HIGH-RESOLUTION INFRARED IMAGING AND SPECTROSCOPY OF THE PISTOL NEBULA: EVIDENCE FOR EJECTION[1]

DONALD F. FIGER,[2,3] MARK MORRIS,[2,4] T. R. GEBALLE,[5] R. MICHAEL RICH,[2] EUGENE SERABYN,[6] IAN S. MCLEAN,[2] R. C. PUETTER,[7] AND AMOS YAHIL[8]

Received 1999 February 19; accepted 1999 June 24

ABSTRACT

We present new infrared images, obtained with the *Hubble Space Telescope* (*HST*) Near-Infrared Camera and Multiobject Spectrometer (NICMOS), and Brα (4.05 μm) spectroscopy, obtained using CGS4 on UKIRT, of the Pistol Star and its associated nebula. We find strong evidence to support the hypothesis that the Pistol Nebula was ejected from the Pistol Star. The Paα (1.87 μm) NICMOS image shows that the nebula completely surrounds the Pistol Star, although the line intensity is much stronger on its northern and western edges. The Brα CGS4 spectra show the classical ringlike signature of quasi-spherical expansion. The blueshifted emission ($V_{max} \approx -60$ km s^{-1}) is much weaker than the redshifted emission ($V_{max} \approx +10$ km s^{-1}), where the velocities are with respect to the velocity of the Pistol Star; further, the redshifted emission spans a very narrow range of velocities, i.e., it appears "flattened" in the position-velocity diagram. These data suggest that the nebula was ejected from the star several thousand years ago, with a velocity between the current terminal velocity of the stellar wind (95 km s^{-1}) and the present expansion velocity of gas in the outer shell of the nebula (60 km s^{-1}). The Paα image reveals several emission-line stars in the region, including two newly identified emission-line stars north of the Pistol Star, both of which are likely to be the hottest known stars in the Galactic center with spectral types earlier than WC8 and $T_{eff} > 50{,}000$ K). The presence of these stars, the morphology of the Paα emission, and the velocity field in the gas suggest that the side of the nebula farthest from us is approaching, and being ionized by, the hot stars of the Quintuplet and that the highest velocity redshifted gas has been decelerated by winds from the Quintuplet stars. We also discuss the possibility that the nebular gas might be magnetically confined by the ambient magnetic field delineated by the nearby nonthermal filaments.

Subject headings: Galaxy: center — infrared: ISM: continuum — infrared: ISM: lines and bands — ISM: individual (G0.15−0.05)

1. INTRODUCTION

The Pistol H II region (Yusef-Zadeh & Morris 1987) surrounds one of the most luminous stars known, the "Pistol Star" (Figer et al. 1998, hereafter F98). Located near the Galactic center ($l, b = +0.15, -0.05$), the nebula appears to be elongated parallel to, and precisely bounded by, two prominent filaments of the Radio Arc in the Galactic center. The apparent coincidence of the Pistol Nebula and the nearby Sickle H II region (G0.18−0.04) with the nonthermal radio filaments has prompted several groups to consider that gas in the H II regions might be ionized by the relativistic particles in the filaments (Yusef-Zadeh & Morris 1987; Serabyn & Güsten 1991). Moneti, Glass, & Moorwood (1994) first identified the "Pistol Star," their "serendipitous source," noting its strong Brγ emission. Cotera et al. (1994) independently identified the same star as "Pistol Source A," suggesting that it might be responsible for ionizing the Pistol Nebula (see also Harris et al. 1994). Figer, McLean, & Morris (1995, hereafter FMM95) and Figer, McLean, & Morris (1999, hereafter FMM99) proposed that the star is a luminous blue variable (LBV) and that the nebula is photoionized by the nearby large population of extremely massive, luminous stars, some of which are Wolf-Rayet stars, in agreement with Timmermann et al. (1996). FMM95 further proposed that the Pistol Nebula is circumstellar ejecta from the Pistol Star; note that the Pistol Star has the same line-of-sight velocity as the Pistol Nebula (Figer 1995; Yusef-Zadeh, Morris, & van Gorkom 1989).

F98 find that the Pistol Star is extremely luminous ($L > 10^{6.6}\ L_{\odot}$; also see FMM95 and Cotera et al. 1996), with no evidence of a comparably bright companion to within 14 mas (110 AU). F98 argue that the star is a luminous blue variable ("LBV"; Conti 1984; Humphreys & Davidson 1994), given the star's position in the H-R diagram, placement within the Pistol Nebula, and near-infrared spectrum (also see FMM95). Most stars in the LBV class are surrounded by circumstellar ejecta (Nota et al. 1995), and P. S. Conti (1997, private communication) has suggested that these nebulae should be regarded as identify-

[1] Based on observations with the NASA/ESA *Hubble Space Telescope*, obtained at the Space Telescope Science Institute, which is operated by the Association of Universities for Research in Astronomy, Inc. under NASA contract NAS5-26555.

[2] Division of Astronomy, Department of Physics and Astronomy, University of California, Los Angeles, 405 Hilgard Avenue, Los Angeles, CA 90095-1562; figer@astro.ucla.edu, morris@astro.ucla.edu, rmr@astro.ucla.edu, mclean@astro.ucla.edu.

[3] Space Telescope Science Institute, 3700 San Martin Drive, Baltimore, MD 21218.

[4] Institut d'Astrophysique de Paris, 98 bis Blvd Arago, 75014 Paris, France.

[5] Gemini Observatory, 670 North A'ohoku Place, Hilo, HI 96720; tgeballe@gemini.edu.

[6] JPL 171-113, 4800 Oak Grove Drive, Pasadena, CA 91109; eserabyn@huey.jpl.nasa.gov.

[7] Center for Astrophysics and Space Sciences, University of California, San Diego, 9500 Gilman Drive, La Jolla, CA 92093-0111; rpuetter@ucsd.edu.

[8] Department of Physics and Astronomy, State University of New York at Stony Brook, Stony Brook, NY 11794-3800; Amos.Yahil@sunysb.edu.

ing characteristics of the class. Recent photometric monitoring by Glass et al. (1999) has confirmed that the Pistol Star is photometrically variable by ≈ 0.5 mag in the K band.

This paper provides new evidence that the Pistol Nebula is photoionized circumstellar ejecta emitted by the Pistol Star, although we argue that the nebula is primarily ionized by nearby hot stars elsewhere in the Quintuplet cluster. We present *HST*/NICMOS Paα (H I 3–4, 1.87 μm) images that reveal the Pistol Nebula in new detail and show that the nebula completely surrounds the Pistol Star. We present Brα (H I 4–5, 4.05 μm) spectroscopy that shows that the ionized gas in the nebula has a velocity structure characteristic of quasi-spherical expanding systems, such as planetary nebulae. We propose that the Pistol Star is an extremely luminous LBV surrounded by a massive ejection nebula that is primarily ionized externally by nearby hot stars and that is physically interacting with the strong winds of these stars.

2. OBSERVATIONS

2.1. *NICMOS Imaging*

The imaging data were obtained using *HST*/NICMOS. A 2×2 NIC2 mosaic was obtained on UT 1997 September 13/14 in the F187N ($\lambda_{\rm center} = 1.87$ μm, Paα) and F190N ($\lambda_{\rm center} = 1.90$ μm, continuum) filters with 19.″05 spacing between images; the plate scale was 0.″076 pixel^{-1} (x) by 0.″075 pixel^{-1} (y), in detector coordinates. The STEP256 sequence was used in the MULTIACCUM read mode with 11 reads, i.e., the exposure time was ≈ 256 s per image. The pattern was centered on R.A. $17^{\rm h}$ $43^{\rm m}$ $5^{\rm s}.0$, decl. -28° 48′ 54.″87 (B1950) with an orientation of $-134.^\circ7$. The names of the data files are given in Table 1. The data were reduced with STScI pipeline routines, calnica and calnicb, using the calibration files listed in Table 2.

The color composite image in Figure 1 was produced with calibration files available at the time of the observations. In this figure, the difference of the F187N and F190N images was coded as red, the F190N image as blue, and the F187N image as green. A recalibration was used to produce the other figures and to extract the photometry, as described below. The second calibration used more recent files, most notably, on-orbit flat field images. Figure 2 shows a negative gray-scale image of the difference frame (F187N − F190N).

TABLE 1

SUMMARY OF OBSERVATIONS

Position	F187N Data Set	F190N Data Set
N	N44T01K6	N44T01K9
E	N44T01KC	N44T01KF
S.....	N44T01KJ	N44T01KM
W	N44T01KP	N44T01KS

2.2. *Spectroscopy*

Spectra in the Brα region were obtained with the cooled grating spectrometer, CGS4, on the United Kingdom Infrared Telescope (UKIRT) on UT 1998 July 5, July 10, and August 3. The echelle grating and the 300 mm focal length camera were used to produce a plate scale of 0.″45 × 0.″85 pixel^{-1} (width × height). The width of the slit was 2 pixels (0.″90), and its length was approximately 80″. The final spectra were constructed from sets of four exposures, taken after sequentially translating the detector array by 0.5 pixel with respect to the spectrum produced by the fixed slit and grating. The final reconstructed spectra have an effective resolving power of $\approx 16{,}000$ ($\Delta V_{\rm res.\ elt} \approx 19$ km s^{-1}). The slit was oriented north-south on July 5 and east-west on July 10, with the Pistol Star near the middle of the slit on both occasions. On August 3, two additional spectral images were obtained, one with the slit at a position angle of 115° and centered at R.A. = $17^{\rm h}$ $43^{\rm m}$ $5^{\rm s}.16$, decl. = -28° 48′ 45.″1 (B1950) to extend along the "barrel" of the Pistol, the other with the slit at a position angle of 25° and centered at R.A. = $17^{\rm h}$ $43^{\rm m}$ $3^{\rm s}.90$, decl. = -28° 48′ 50.″3 (B1950) to lie along the "handle" of the Pistol (see Fig. 2). The telescope was nodded well off of the nebula to obtain "blank sky" images for subtraction. The on-source integration times were 240 s on July 5, 768 s on July 10, and 240 and 480 s, respectively, for the August 3 positions. The seeing was poor (1.″5 FWHM) on July 5 and was subarcsecond on the other two nights.

Data reduction was accomplished using the CGS4 on-line software augmented off line by the Figaro data reduction package maintained by the Starlink Project. Bad pixel removal, flat-fielding, and co-adding of object-sky frame pairs were performed to produce the final spectral images. The spectrum of the Pistol Star was extracted and then divided by a similarly extracted spectrum of the nearby Quintuplet star, "q3" (nomenclature from Moneti et al. 1994), which is featureless in this spectral region (see Fig. 1 in F98).

The wavelength scales were determined by observing hydrogen and helium emission lines from the planetary nebula NGC 6572 and converted to the local standard of rest (LSR) frame (Schneider et al. 1983). The final reduced

TABLE 2

CALIBRATION IMAGES

Calibration	Original Calibration	Final Calibration
Mask	H4214599N	H4214599N
Noise	H4216218N	H4216218N
Linearity	H3V1404NN	H4N1654BN
Dark	H7B1528ON	HAD12034N
Flat[a]	H1S1337HN/H1S1337JN	I3A1616AN/I3A1616BN
Photometric table.....	H7M1005JN	I3G1220AN
Illum[a]	H2413241N/H2413243N	H2413241N/H2413243N

[a] F187N/F190N.

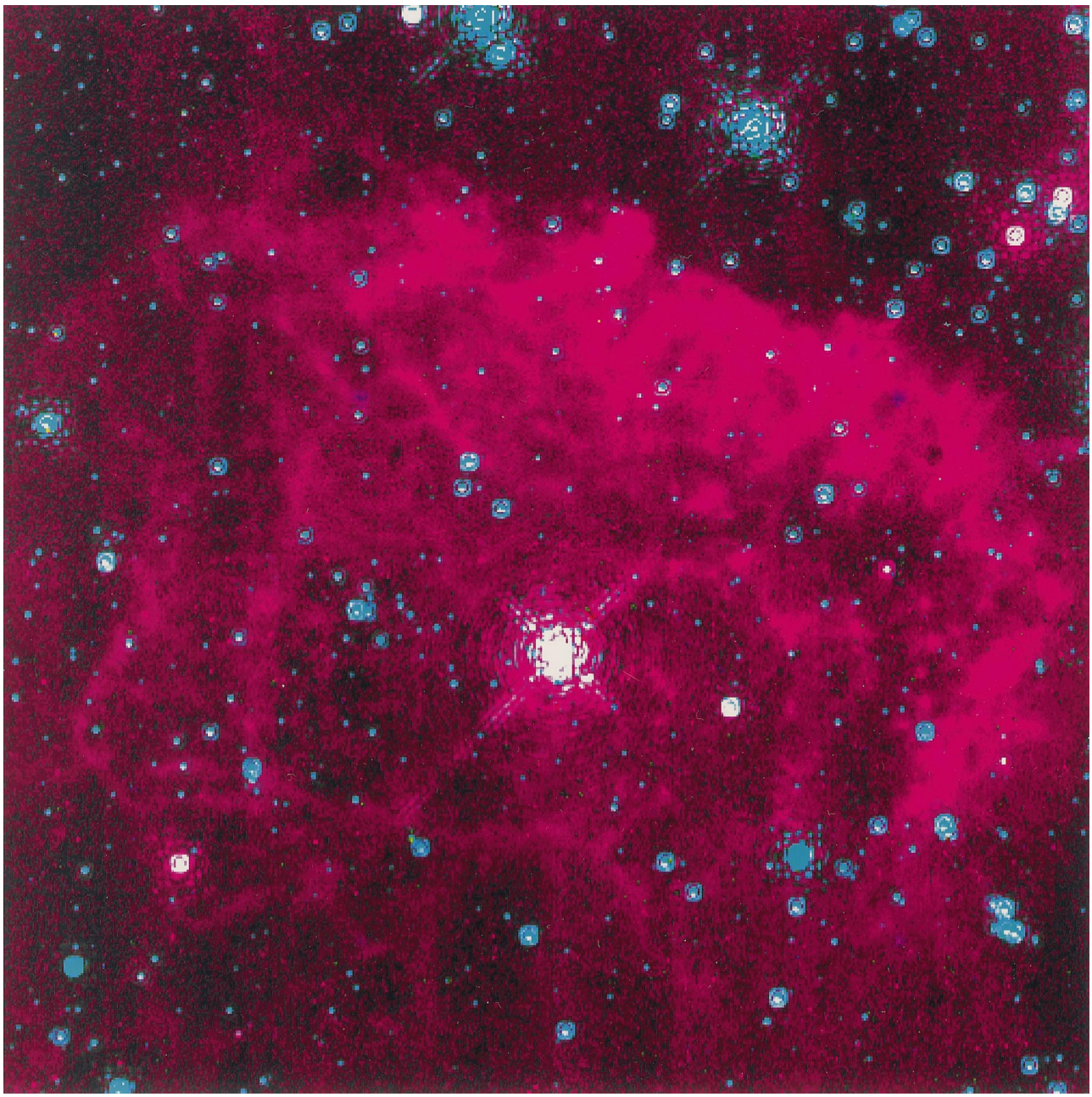

FIG. 1.—Color composite of the F187N minus F190N image (*red*), the F190N image (*blue*), and the F187N image (*green*). The reddish hue reveals ionized hydrogen gas recombining through the $n = 4$ to $n = 3$ transition. The plate scale for all images is 0.″076 pixel^{-1} in x and 0.″075 pixel^{-1} in y. Pixel (253,254.5) corresponds to the center of the mosaic; see text and Fig. 2 legend for coordinates.

spectrum of the Pistol Star obtained on July 10 is shown in Figure 3. Portions of the wavelength-calibrated spectral images are shown in Figures 4*a*–4*d*.

3. ANALYSIS AND RESULTS

The data have been analyzed in a variety of ways. First, we extracted photometry from the emission-line and continuum images using DAOPHOT and the Pixon reconstructed data (which will be discussed in detail in § 3.2), preferring the latter method for extracting the estimate for the nebular flux. Second, we examined the continuum image (F190N) for possible companions to the Pistol Star. Third, we estimated the extinction along the line of sight to the nebula and the mass of ionized gas in the nebula using the continuum-subtracted image which was processed using the Pixon method. Fourth, using this same image, we extracted point-source photometry in order to obtain the 1.87 μm flux excesses for the emission-line stars in the region. Last, we used the nebular spectra to extract the crucial velocity information that suggests an expanding nebula. We assume $d_{GC} = 8000$ pc (Reid 1993) throughout the paper.

3.1. *Photometry*

The photometry was performed using two methods. First, the Pixon deconvolution method (see below) was used to estimate the flux from the Pistol Star in an infinite aperture from the originally calibrated data. Second, the

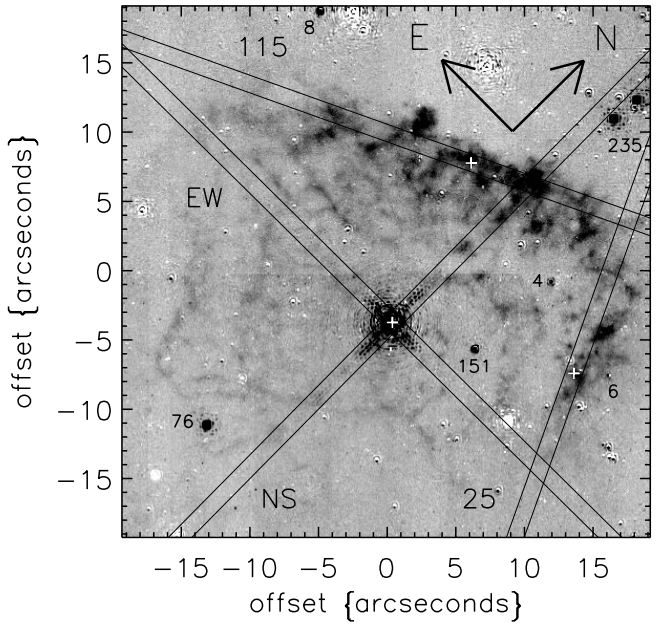

FIG. 2.—Negative gray-scale image of the continuum-subtracted flux in the narrow band F187N filter ($\lambda = 1.87\mu$m). The Pistol Nebula, Pistol Star (near center), and several emission-line stars can clearly be seen. The longest emission ridge near the top of the figure is the "barrel," while the short emission ridge to the right is the "handle." Nomenclature from FMM99 is used for previously identified emission-line stars; the numbering from Table 4 is used for newly identified emission-line stars. The pair of stars labeled "235" are referred to as 235N and 235S in the text. Slit positions on the nebula are indicated and labelled according to their positional angle on the sky; plus signs are at the slit centers.

DAOPHOT package in IRAF[9] was used to extract the number of counts in a 0.″5 radius aperture from the newly calibrated images; this value was then multiplied by 1.228 to simulate an infinite radius aperture. We find that this factor is appropriate, given the PSF profile measured in our data and shown in Figure 5. Results from both methods are

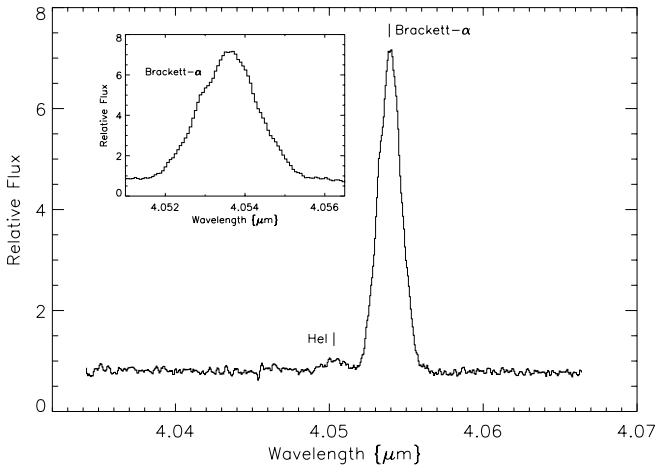

FIG. 3.—High-resolution spectrum ($R \approx 16{,}000$) of the Pistol Star near the Brα line. Zero velocity corresponds to the velocity of peak line emission in the star.

[9] IRAF is distributed by the National Optical Astronomy Observatories, which are operated by the Association of Universities for Research in Astronomy, Inc., under cooperative agreement with the National Science Foundation.

TABLE 3

PHOTOMETRY

Method	F_{F187N} (W cm^{-2} μm^{-1})	F_{F190N} (W cm^{-2} μm^{-1})
Pixon[a]	6.22(10^{-17})	4.12(10^{-17})
DAOPHOT[b].....	6.24(10^{-17})	4.14(10^{-17})

[a] A 0.″375 radius aperture was used to sum the counts. The zero points are 4.336(10^{-18}) ergs cm^{-2} Å^{-1} DN^{-1} for F187N and 4.293(10^{-18}) ergs cm^{-2} Å^{-1} DN^{-1} for F190N.

[b] A 0.″5 radius aperture was used to sum the counts, and the result was multiplied by 1.228, as indicated by our analysis of the PSF in the images. The zero points are 3.537(10^{-18}) ergs cm^{-2} Å^{-1} DN^{-1} for F187N and 3.519(10^{-18}) ergs cm^{-2} Å^{-1} DN^{-1} for F190N.

shown in Table 3; they differ by an insignificant amount. The flux at 1.90 μm compares favorably with the value implied by fitting a curve through the reddened spectral energy distribution in Figure 9 of F98, $\approx$3.9(10^{-17}) W cm^{-2} μm^{-1}; however, this might just be a coincidence, given that the star is variable (Glass et al. 1999).

3.2. *Pixon Image Reconstruction*

The Pixon method's approach to deconvolution is to minimize the χ^2 fit to the data of a minimum complexity, multiresolution image model (see Piña & Puetter 1993; Puetter 1995; Puetter & Yahil 1999). Relative to competing methods, use of a minimum complexity image model results in a wide range of benefits, including increased spatial resolution, decreased artifacts, and increased sensitivity to faint sources otherwise hidden by these artifacts. The Pixon method models the image as a local convolution of a smoothing function and a pseudoimage. The pseudoimage contains all of the flux in the image while the smoothing functions decrease the complexity of the image model by introducing at each point in the image the maximum allowable correlation between image points. A Pixon reconstruction iterates between calculating the pseudoimage given a set of smoothing kernels and calculating the largest smoothing kernel acceptable at each location in the image given the current pseudoimage. Iteration proceeds until convergence, and no stopping criterion is required. Usually only a few (two or three) iterations between pseudoimage and smoothing kernel calculation are required for convergence.

The PSF used in the reconstruction was determined iteratively, and the resulting image is shown in Figure 6. The data profile around the Pistol Star itself was used as an initial guess for the PSF, and this PSF was then used to perform an image reconstruction of the entire field. Next, using the relative brightnesses of additional stars in the field and their determined centroids, a second, improved PSF was calculated from the data by reversing the roles of image and PSF. (Recall that a convolution integral is invariant under the interchange of its components, i.e., the image and the PSF.) This produced a new PSF that was used to perform a second image reconstruction of the field. The second PSF was clearly a significant improvement over the first PSF, but inspection of the second reconstruction revealed the presence of weak field stars in the wings of the Pistol Star that clearly contributed to artifacts in the wings of the PSF estimate. These were removed by hand by subtracting the current PSF scaled to the brightness and position of the offending stars, and the whole process was repeated. A new reconstruction was performed, a third PSF

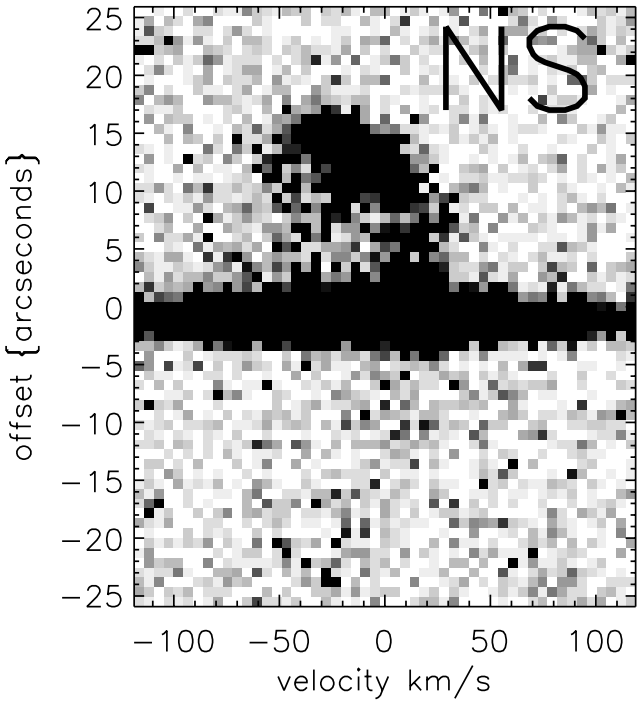

FIG. 4*a*

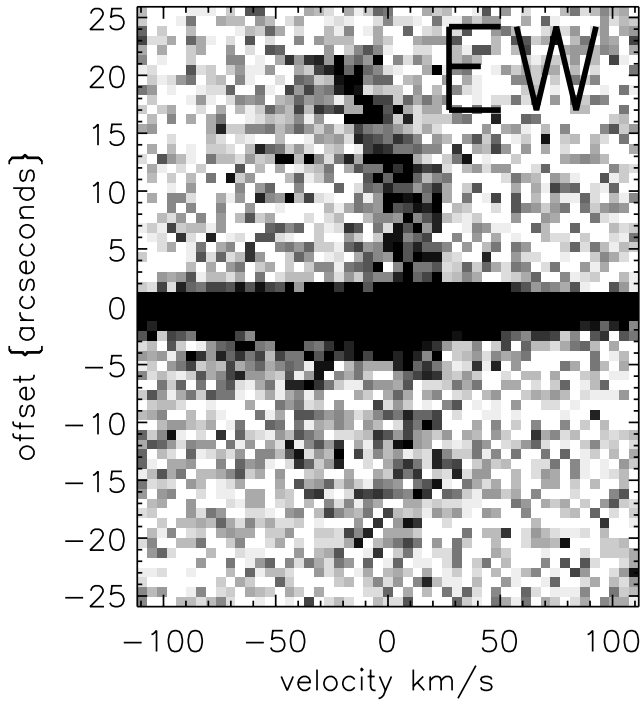

FIG. 4*b*

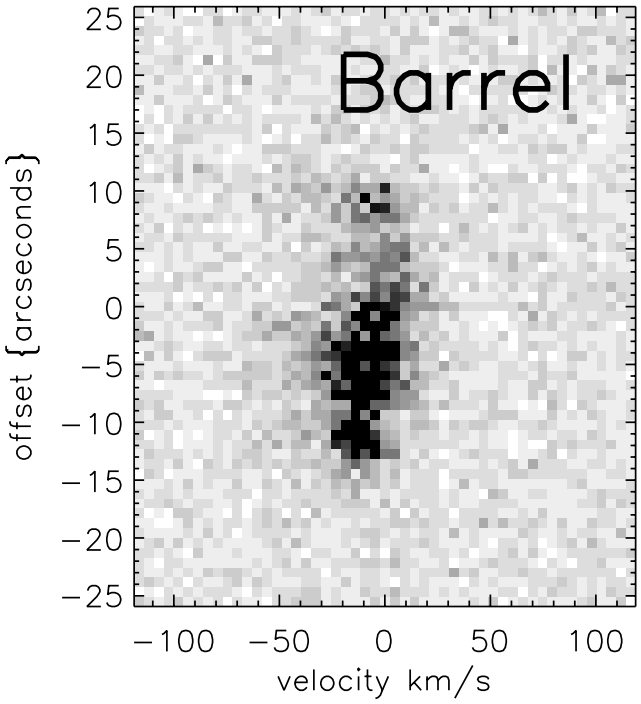

FIG. 4*c*

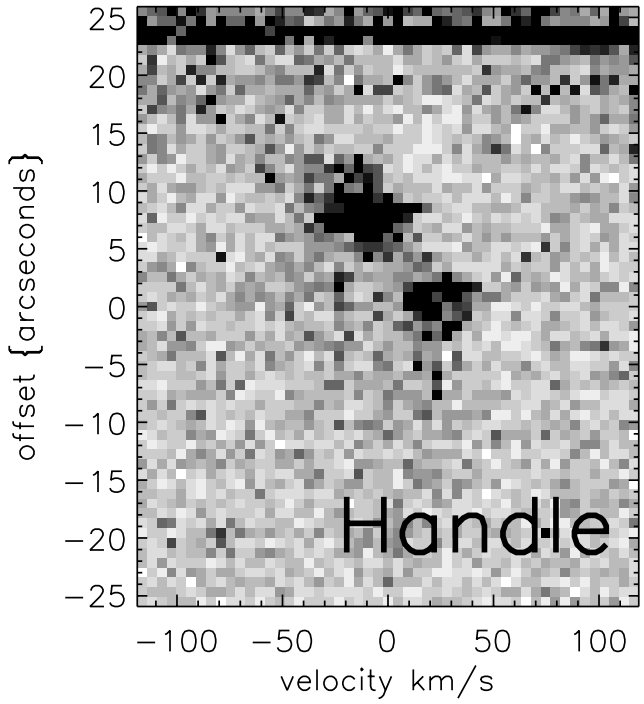

FIG. 4*d*

FIG. 4—(*a*) Long-slit spectrum of the Pistol Star and associated nebula with the slit oriented NS as indicated on Fig. 2. North is up, and positive velocity indicates a redshift. The velocity zero point corresponds to the peak of the Brα line in the Pistol Star, $\approx +130$ km s^{-1}. The origin of the spatial scale (y-axis) for this figure and (*b*)–(*d*) is indicated by a plus sign on the slit positions shown on Fig. 2. Notice the elliptical envelope of the emission, consistent with an expanding nebula. (*b*) Long-slit spectrum of the Pistol Star and nebula with slit oriented east-west (Fig. 2); east is up. Axes as in (*a*). Notice the nearly complete ellipse of emission, consistent with an expanding nebula. (*c*) Long-slit spectrum of the "barrel" of the nebula (Fig. 2). The slit was oriented with PA = 25°. Southeast is up. (*d*) Long-slit spectrum of the "barrel" of the nebula (Fig. 2). The slit was oriented with PA = 115°. Northeast is up. The spectrum near the top of the image is due to an emission line star.

determination was made, and a second weak point source removal was performed by hand. This last iteration produced essentially no change in the PSF core and only minor changes in its wings, so this final PSF was adopted.

The Pixon image of the F187N (Paα) mosaic has a dynamic range $\sim 3(10^5)$, well beyond the human perceptual capability, so the brighter stars were saturated to allow the fainter stars plus nebula to take up most of the displayed

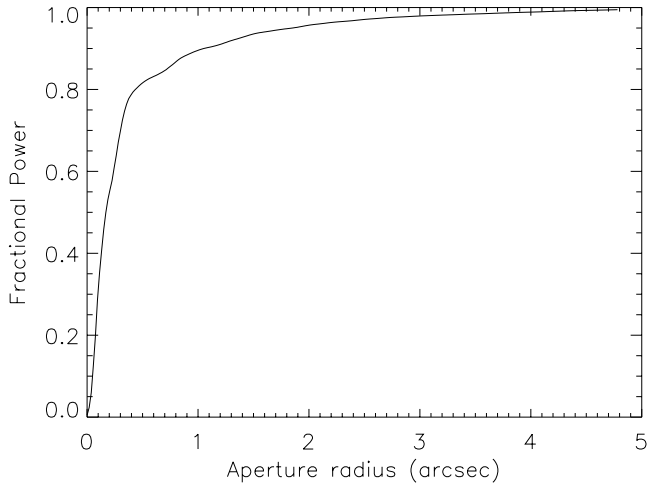

FIG. 5.—Plot of enclosed energy as a function of aperture radius for PSF in the F190N filter.

dynamic range. The statistical significance of faint structures in the image can be estimated from the residual errors. Since a Pixon reconstruction is made up of smooth Pixon elements, correlated on the scale of the kernel function, the signal-to-noise ratio in the reconstruction is measured per Pixon element and not per pixel. Computed in this way, the faintest parts of the nebula (well off its brighter parts) have SNR ≥ 10 with a typical SNR ~ 30.

The most important feature of the reconstruction, however, is the removal of the diffraction spikes of the stars. The diffraction sidelobes of the Pistol Star itself have been successfully removed to about one part in 10^5 in its immediate vicinity, with the exception of a few artifacts discussed below. Specifically, the reconstructed Pistol Star has nearly all of its flux in a 3×3 pixel box (0.″106 radius) with the central pixel containing 74% of the total flux. This is to be compared with the data, where 47% of the flux extends beyond a radius of 0.″225, 20% outside of a radius of 0.″375, and 9% outside of a radius of 2.″4. However, a small amount of remaining diffracted light from the Pistol Star does remain in the reconstruction where the diffraction spikes run into the nebular emission at a radius of 6.″9, too far for an accurate estimate of the PSF.

One of the principal advantages of the Pixon method for crowded fields is that it allows accurate photometry by disentangling the emission for individual sources that has been blended together by PSF blurring. This is especially important in the case of the Pistol Star where a significant fraction of the flux has blended with the nebular emission and with that of nearby stars. Photometry on the reconstructed image need include only the immediate area around any object of interest (e.g., a few pixels on either side). The relative photometric accuracy is limited in bright stars by systematic errors to a precision of roughly 1% of the total flux in individual point sources. For fainter stars, photon counting statistics and read noise will dominate photometric errors. The 1% error for bright stars has contributions from two primary sources. First, low-level artifacts arising from an imperfect PSF estimate can be seen surrounding several of the brighter stars. Second, inspection of the residual errors (data minus the PSF convolved with the reconstructed image) shows the presence of low-level features from an imperfectly removed diffraction pattern (first

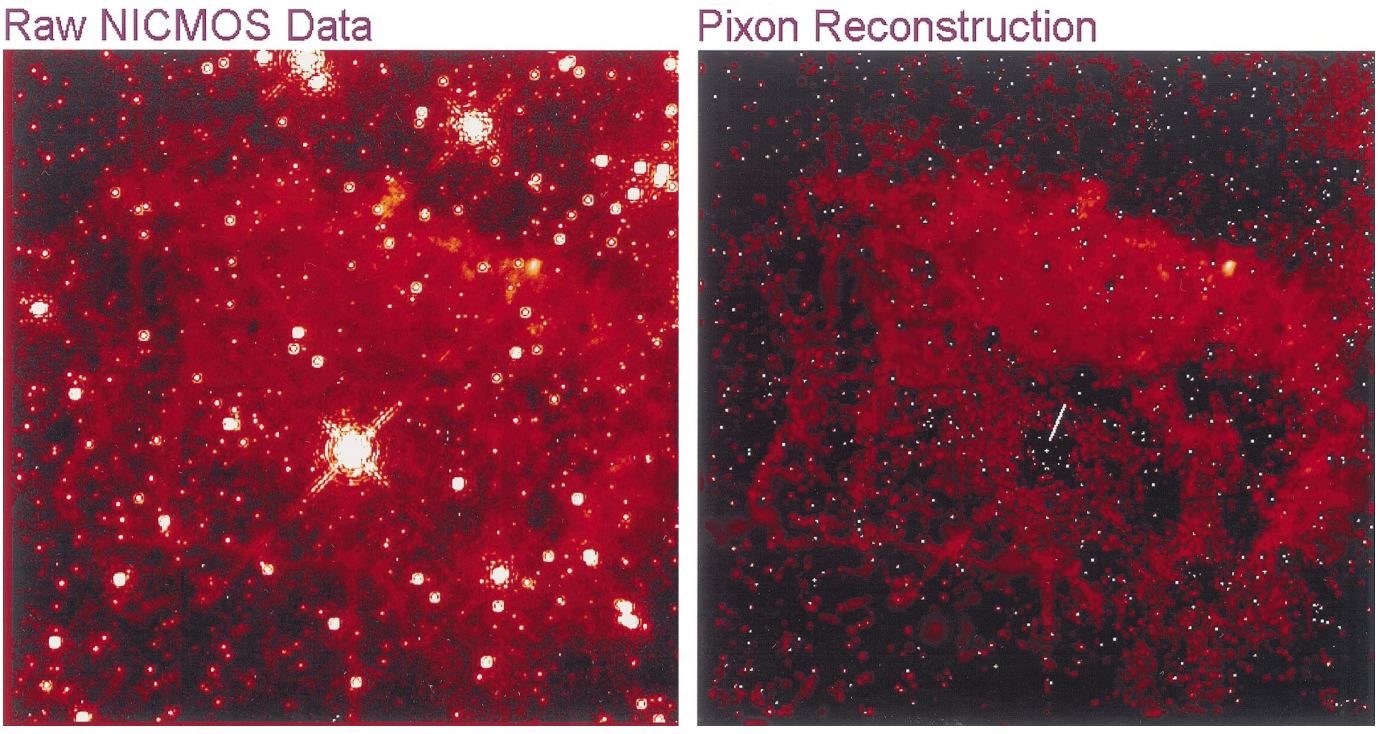

FIG. 6.—Comparison of the unprocessed and Pixon-reconstructed Paα image of the Pistol star. The nebular emission (maximum value 0.9 data units) is displayed raised to the 0.6 power in both the raw and reconstructed images. Owing to the high dynamic range of the stellar emission, it is treated a little differently for the two images. In the raw image it is simply saturated at 1 data unit and then raised to the 0.6 power. In the reconstructed image, stellar emission is first segmented by finding all pixels whose emission exceeds that of a 5×5 median-filtered reconstruction image by 0.5 data units. The stellar emission is then multiplied by 0.5, saturated at 1 data unit, and raised to the 0.6 power. Around the six brightest stars, three to five residual artifacts were noted in the reconstruction, all within 5 pixels from the positions of the stars and at the same position angles with respect to the stars. These artifacts, whose combined fluxes are $\sim 1\%$ of the total fluxes of the stars, were removed by hand from the reconstruction shown in the figure.

few Airy rings). Nonetheless, the Pixon reconstruction recovers significantly more flux than found by other methods, e.g., DAOPHOT. A number of artifacts are also obvious in the Pixon reconstruction, i.e., "holes" dug out around some of the stars. Their origin lies in the fact that not all stars are centered in the data pixel grid in the same manner. Since the PSF used in the reconstruction must necessarily assume some location for the point source center, stars that are centered differently cannot be precisely reconstructed. The PSF centering selected here was for optimal reconstruction of the Pistol Star since it had the largest diffraction spikes. Consequently, stars centered substantially differently than the Pistol Star cannot be reduced to a point source. To fit the required centroid of the star correctly, their central peaks are broken into a number of pixels. However, this makes the wings of the star too broad. If this profile were to be subtracted from the data, a negative hole would result centered on the star. However, the Pixon method requires nonnegative data. So a somewhat broader hole with flux values near zero intensity is created. Such artifacts can be removed only by performing a reconstruction in which the image resolution is considerably higher than the data pixel grid. Such a reconstruction was not performed here since there was no reliable method of obtaining the PSF on a commensurately fine scale. Also apparent in the Pixon reconstruction are low signal-to-noise ratio "blobby" structures. These occur especially around bright stars. These features result from incompletely reconstructed starlight from the bright stars owing to errors in the determination of the appropriate PSF for the stars in question. These errors can arise from a number of sources. A primary error is due to different centering of the PSF and the star in question. Both of these error sources are discussed above. The presence of these "blobby" is especially obvious around the Pistol Star itself and near some of the stars near the northern end of the western border of the frame.

Closer in (i.e., at small radii) to the stars showing surrounding "blobby" structure, the PSF is more completely removed in the reconstruction. There is a noticeable "hole" in emission, for example, close to the Pistol Star (within a 1.″5 radius). This emission has been reconcentrated back into the central pixel of the Pistol Star in the reconstruction. Of course weak nebular emission might also be mistakenly recollected back into the Pistol Star from this region since it is very difficult to distinguish leaked stellar power (owing to PSF misalignment) and low-level nebular emission so close to the Pistol Star. Any such emission, however, would affect the estimated flux for the Pistol Star at a very low level ($\ll 1\%$).

3.3. *Stellar Image*

The *HST* image can be used to find coordinates for the Pistol Star. Our astrometry gives R.A. $17^{h}\ 43^{m}\ 4^{s}.85 \pm 0^{s}.1$, decl. $-28^{\circ}\ 48'\ 57''.23 \pm 1''$ (B1950), as compared to the coordinates from Lang et al. (1999) of R.A. $17^{h}\ 43^{m}\ 4^{s}.77 \pm 0^{s}.01$, decl. $-28^{\circ}\ 48'\ 57''.0 \pm 0''.1$ (B1950). The errors for the *HST* position are dominated by systematic errors in determining the coordinates for the guide stars used in setting the header values in the images. These astrometry agree with those in Nagata et al. (1993): R.A. $17^{h}\ 43^{m}\ 4^{s}.8$, decl. $-28^{\circ}\ 48'\ 57''$ (B1950).

The high resolution of the images shows that the Pistol Star is single on scales greater than ≈ 800 AU (0.″1), consistent with the much smaller limit of 110 AU in F98. Figure 7 shows the immediate vicinity of the Pistol Star in the F190N image. The first Airy ring is revealed, but no noticeable companions can be seen, and the limit on the flux of any companion is 10% of the flux of the Pistol Star. The contrast in brightness is greater than 10 to 1 between the brightest pixel on the peak and the brightest pixel in the Airy ring. As further evidence for the star being single, the Pistol Star provided the best point-spread function in the field for the Pixon deconvolution.

3.4. *Nebular Morphology, Flux, and Mass*

Figures 1 and 2 show that the nebula completely surrounds the Pistol Star, although it is quite faint on the southern and eastern portions. The nebula is dominated by roughly rectangular, concentric shells having sizes of 0.8×1.2 pc and 0.4×0.6 pc, and both major axes oriented 45° west of north. Note that their intensity characteristics differ in that the brighter outer ring has strong brightness asymmetries. There also appear to be two opposing lines of emission extending to the north and south of the star that are coincident with diffraction spikes from the star. The northern line terminates in a bright knot of emission (the "northern knot"), where the nebula has its highest surface brightness flux density. Although this string of knots lies along a diffraction spike associated with the Pistol Star, the flux in the string is ≈ 10 times greater than the flux expected from the diffraction spike at its distance from the star, and the string does not show the three-line pattern of the spike. In addition, the string is clearly seen in the radiograph of Figure 13 in F98. There are also stringlike features and other knots in the northern ridge (the "barrel"; PA = 115°) and the western ridge (the "handle"; PA = 25°).

The extinction along the line of sight to the nebula can be estimated by comparing the Paα flux to free-free emission at 6 cm. After subtracting flux from stars, we calculate $F_{\mathrm{Pa}\alpha} = 3.1(10^{-19}) \pm 1.1(10^{-20})$ W cm^{-2} integrated over the nebula; the uncertainty is set by the estimate of background flux. Lang, Goss, & Wood (1997) find 0.5 Jy from the nebula at 6 cm. Using the relation between $I_{\mathrm{Br}\gamma}$ and $I_{6\ \mathrm{cm}}$ in Wynn-Williams et al. (1978), and $I_{\mathrm{Pa}\alpha}/I_{\mathrm{Br}\gamma} = 12.5$ (Hummer & Storey 1987) for $T_e = 5000$ K and $n_e = 500$ cm^{-3} (Lang et al. 1997), we find $A_{1.87\mu\mathrm{m}} = 3.8 \pm 0.3$. This is equivalent to $A_K = 2.9 \pm 0.3$ assuming $A \propto \lambda^{-1.6}$ (Rieke, Rieke, & Paul 1989). This value is consistent with $A_K = 3.2 \pm 0.5$ estimated in F98 for the Pistol Star.

We may now estimate the ionized gas mass:

$$M_{\mathrm{ionized}} = \rho_{\mathrm{ionized}} V\ , \tag{1}$$

where ρ_{ionized} is the density of ionized gas and V is the emitting volume. We model the emitting volume as a spherical shell with inner radius, r_i, and outer radius, r_o, i.e.,

$$V = \tfrac{4}{3}\pi(r_o^3 - r_i^3)f\ , \tag{2}$$

where f is the fraction of the shell that is ionized and accounts for incomplete ionization of ejecta in the shell and an asymmetric external ionizing field. The density is $m_p\langle n_e^2\rangle^{1/2}$, where m_p is the mass of a proton, and $\langle n_e^2\rangle^{1/2}$ is deduced from the volume emissivity for free-free emission, $j_{\nu,\mathrm{ff}}$, and the measured flux, F_ν:

$$F_\nu = \frac{j_{\nu,ff}\,V}{4\pi d^2}\ , \tag{3}$$

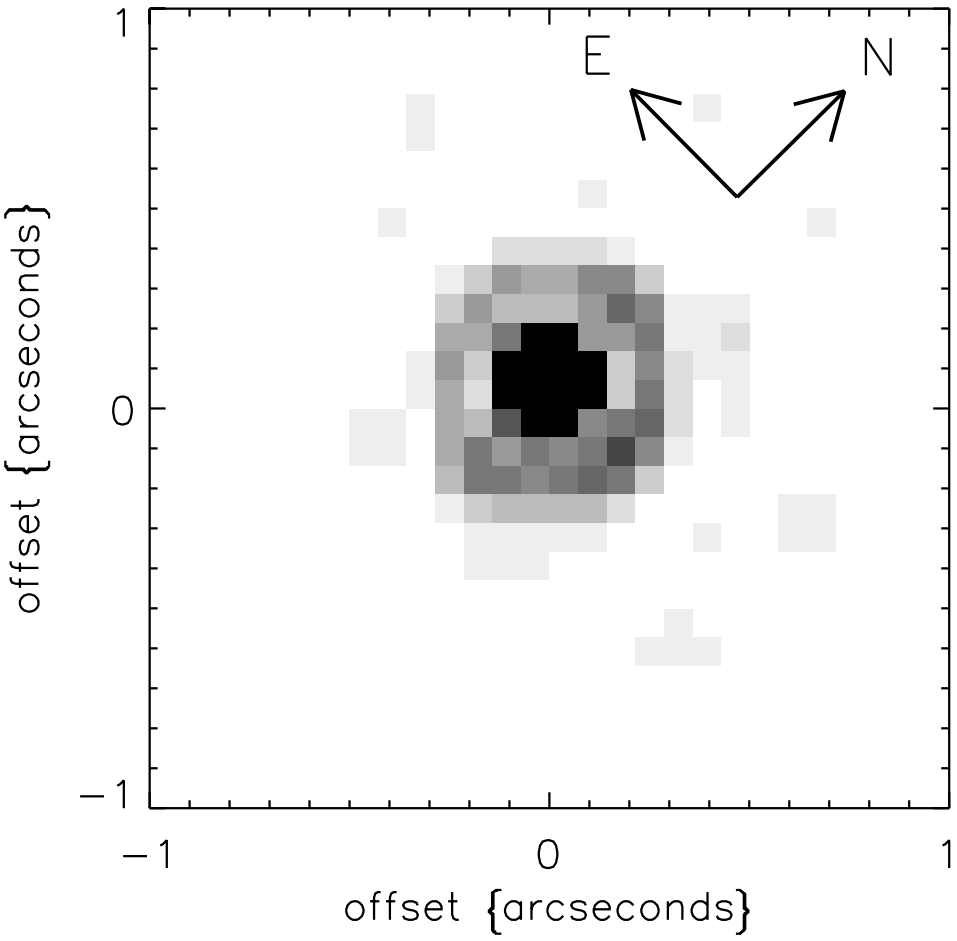

FIG. 7.—Log stretch of central 1″ × 1″ region surrounding the Pistol Star. The first Airy ring can clearly be seen, and there is no evidence of a bright companion. The brightest pixel on the peak has 10 times the flux of the brightest pixel in the Airy ring.

where d is the distance between the Earth and the object. The volume emissivity in the Rayleigh-Jeans limit is

$$j_{\nu,\mathrm{ff}} = 0.018 \frac{\langle n_e^2 \rangle}{T_e^{3/2}} \frac{1}{\nu^2} g_{\nu,\mathrm{ff}} B_{\nu,T_e} \text{ ergs cm}^{-3} \text{ s}^{-1} , \quad (4)$$

where T_e is the electron temperature, $g_{\nu,\mathrm{ff}}$ is the Gaunt factor, B_{ν,T_e} is the Planck function, and all quantities are in cgs units. Combining equations (3) and (4), we find

$$\langle n_e^2 \rangle = \frac{4\pi d^2}{V} \frac{\nu^2 T_e^{3/2}}{0.018 g_{\nu,\mathrm{ff}} B_{\nu,T_e}} F_\nu \text{ cm}^{-6} . \quad (5)$$

Using this formulation, we find $V = 0.19$ pc^3, $\langle n_e^2 \rangle^{1/2} = 1200$ cm^{-3}, and $M_{\mathrm{ionized}} = 5.6\ M_\odot$, assuming $r_o = 0.60$ pc, $r_i = 0.50$ pc, $T_e = 3600$ K, and $g_{\nu,\mathrm{ff}} = 4.2$. The total gas in the ejection, M_{gas}, is then $M_{\mathrm{ionized}}/f = 11\ M_\odot$, assuming $f = 0.5$. The value for the ionized fraction, f, is motivated by the fact that the ionized gas appears to be confined to the northern side of the expanding ejecta (Moneti et al. 1999). The adopted value of r_o is measured directly off the image, and r_i is estimated from the apparent shell thickness. We are also assuming that the thickness of the ionized layer is equal to, or less than, the thickness of the shell.

The dust mass in the nebula can be estimated as follows:

$$M_{\mathrm{dust}} = \left(\frac{F_\nu d^2}{B_{\nu,T_d}} \right) \times A , \quad (6)$$

where F_ν is the measured flux, T_d is the dust temperature, and A is the mass per effective cross section of the dust and is defined in Marston & Dickens (1988).

From Marston & Dickens (1988), $A \approx 0.013$ g cm^{-2} at 60 μm, using their grain model. Taking $F_{60\mu\mathrm{m}} = 600$ Jy and $T = 173$ K (Simpson et al. 1997), we find $M_{\mathrm{dust}} = 0.004\ M_\odot$ and $M_{\mathrm{gas}}/M_{\mathrm{dust}} \approx 2800$. For any reasonable geometry, this dust mass implies $A_V \ll 1$ for the whole nebula (consistent with § 4.3.3 in F98).

3.5. *High-Resolution Spectrum and the Expanding Ring*

Table 4 lists important parameters of the H I 4–5 and He I 4–5 lines in the spectrum (Fig. 3), along with values for those lines from the earlier spectrum in F98; notice that the strength of the Brα line is variable, confirming the behavior of the Brγ line (H I 4–7, 2.166 μm) reported in F98. The Brα line again shows more emission on the blueward side, so that the centroid of emission is shifted blueward from the peak by several km s^{-1}. We interpret the asymmetry in the line as due to the opacity of the approaching (near) side of the wind which blocks emission from the far side of the wind.

We now turn to the velocity field of the nebula, which we have mapped for the first time using the long-slit Brα spectra. Figure 2 shows the slit positions observed, and Figures 4*a*–4*d* show the long-slit spectra; the velocity scale is normalized so that the zero point corresponds to the radial velocity of the Pistol Star, $\approx +130$ km s^{-1} (LSR). The velocity field in both the east-west and north-south slit

TABLE 4

SPECTRAL LINES

Source[a]	Species	λ_{vac} (Å)	V_{LSR} (km s^{-1})	ΔV_{FWHM} (km s^{-1})	W_λ (Å)
This work.....	He I 4–5	40490	107±15	110±30	3.0±0.5
F98	...	...	81±15	...	3.1±0.4[b]
This work.....	H I 4–5	40522.4	126±5	125±10	199±10
F98	...	...	117±15	118±15	150±5

NOTE.—Values were extracted from UT 1998 July 10 data. Uncertainties are given in parentheses.

[a] F98 data were taken from Figer et al. 1998. Note that V_{LOS} given in that paper is equal to $V_{LSR} - 10$ km s^{-1}.

[b] The value in F98 is in error.

positions traces an ellipse, consistent with an optically thin expanding nebula and similar to what is observed in planetary nebulae. The emission is much stronger from the northern and western part of the nebula, consistent with the emission seen in Figures 1 and 2. Referring back to Figure 2, the bright horizontal ridge of emission is called the "barrel" and its emission (Fig. 4*c*) arises mostly from gas near the radial velocity of the Pistol Star. The patchy nature of the emission is evident in Figure 4*d*, the long-slit spectrum of the "handle" of the Pistol Nebula. In general, the redshifted emission is also much stronger than the blushifted part of the ring, which can barely be seen in the images (also see Fig. 6 in F98). The north-south long-slit spectrum (Fig. 4*a*) appears very patchy, with the knot of bright emission toward the north dominating the spectrum (see § 3.4).

Most noteworthy is that our data clearly show the expansion signature and that the expansion ring is asymmetric. The expansion velocity of the nebula cannot be extracted from the spectral images by simply fitting an ellipse because the redshifted emission has a much flatter velocity pattern than the blueshifted emission. The maximum velocity of the blueshifted gas is 60 km s^{-1}, while the maximum velocity of the redshifted gas is 10 km s^{-1}, where both values are with respect to velocity of the Pistol Star. We address the peculiar velocity field of the Pistol Nebula, and its possible origin, in § 4.

Our infrared spectra are consistent with the lower resolution radio data of Lang et al. (1997). They find an average velocity in the H92α line of 115 km s^{-1}, roughly in the middle of the range of gas velocities found in this paper. They were able to split the line profile into two components in the eastern (their Fig. 7*a*) and the southern (their Fig. 11) portions of the nebula. In both cases, the velocities of the fit lines are consistent with the two components we find in our data, i.e., $V_{LSR} \sim 140$ km s^{-1} and $V_{LSR} \sim 70$ km s^{-1}. In other regions, they fit a single line having $\Delta V_{FWHM} \sim 60$ km s^{-1}. Undoubtedly, these single line fits are made to what we now see as two individual lines separated by about 70 km s^{-1} and having very small widths, ~ 10 km s^{-1}.

3.6. *Emission-Line Stars near the Pistol Nebula*

The continuum-subtracted Paα image reveals several emission-line stars (Fig. 2), including stars previously noted (FMM95; FMM99). Table 5 gives the locations and emission-line excesses for the hot stars in the field, where the photometry were extracted from the Pixon reconstructed images.

Equivalent widths can be estimated using equation (7):

$$W_{1.87\,\mu m} = \frac{(F_{F187N} - F_{F190N})}{F_{F190N}} \times \Delta\lambda\,, \qquad (7)$$

where the fluxes are in W cm^{-2} μm^{-1} and $\Delta\lambda$ is the FWHM of the F187N filter (0.0192 μm); this equation assumes that the emission line falls completely within the filter bandwidth. Table 5 includes the equivalent width estimates for the emission-line stars based upon this equation. As a check

TABLE 5

EMISSION-LINE STARS

ID	Other[a]	Sp. Type[a]	R.A.[b] (s)	Decl.[b] (arcsec)	I_{F187N}/I_{F190N}[c]	F_{F190N} (W cm^{-2} μm^{-1})	$W^d_{1.87\,\mu m}$ (Å)	log(Q)	log($L/L_\odot$)
1.....	235S[e]	WC8	4.78	35.51	2.69	$1.17(10^{-18})\pm2.9(10^{-20})$	332	49.8	6.14
2.....	235N[e]	WC8	4.77	33.34	2.27	$1.04(10^{-18})\pm2.8(10^{-20})$	249	49.8	6.12
3.....	76	WC9	5.16	71.91	1.95	$1.01(10^{-18})\pm2.7(10^{-20})$	188	49.5	5.81
4.....	...	...	4.39	46.95	1.52	$1.91(10^{-19})\pm1.2(10^{-20})$	104	...	...
5.....	134	LBV	4.85	57.23	1.50	$4.12(10^{-17})\pm4.1(10^{-19})$	99	<41.5[f]	6.61[f]
6.....	...	...	3.81	48.74	1.24	$1.10(10^{-19})\pm8.7(10^{-21})$	48	...	...
7.....	151	WC8	4.43	54.31	1.21	$1.41(10^{-18})\pm3.2(10^{-20})$	43	49.5	5.96
8.....	...	...	6.31	45.18	1.13	$3.07(10^{-18})\pm4.7(10^{-20})$	28	...	...

NOTE.—Stars were selected if $F_{F187N}/F_{F190N} > 1.10$. Some targets were rejected if their flux ratio appeared to be confused by nebulosity. Lyman continuum fluxes and luminosities for the WC stars are estimated using the new photometry in this paper and the method described in FMM99.

[a] Designations and spectral types are from FMM99. Star 134 is the Pistol Star.

[b] Coordinates are R.A. $+17^h\,43^m$ and decl. $-28°\,58'$ (B1950). The error is 0.01 and 0.1.

[c] $I = F\Delta$; see text. Photometry taken from Pixon reconstructed data.

[d] Equivalent widths are estimated as discussed in the text.

[e] Star 235 was first detected as one object with a spectral type earlier than WC8 (FMM99).

[f] These values are from the "L" model in F98. Note that the "H" model would give log ($L/L_\odot$) = 7.20, and log (Q) = 49.6.

on this relation, note that the equivalent width for the Pistol Star is within 5% of the value given in F98, which was based on a direct spectral measurement. Of course, the star is variable by about half a magnitude in the K band (Glass et al. 1999), so this coincidence might be fortuitous.

3.6.1. *Star 235N and 235S*

The current observations separate star 235 into two emission-line stars having large values of $F_{\rm F187N}/F_{\rm F190N}$. FMM99 observed the two sources as a single star with a spectral type earlier than WC8 ("$<$WC8"). In theory, such stars lack hydrogen, so any emission near 1.87 μm should be attributable to helium lines. Is the 1.87 μm flux from the two stars all due to He II, as would be expected from $<$WC8 stars (Figer, McLean, & Najarro 1997)? We can estimate the expected flux from H I, He I, and He II lines that fall in the F187N filter by scaling the equivalent widths of similar lines in the K-band spectrum in FMM99.

We do not expect any contribution from He I because there are no such lines in the K-band spectrum. The H I contribution can be estimated by scaling the maximum possible contribution to the 2.166 μm line by Brγ. The composite spectrum has $W_{2.166\mu{\rm m}} < 7$ Å. The two stars have similar continuum levels, within 15% at 1.9 μm according to Table 5. Assuming that they have the same continuum flux ratios at 2.166 μm, then the maximum equivalent width for either component in the Brγ line is less than 15 Å. Hummer & Storey (1987) list recombination coefficients that indicate $W_{\rm Pa\alpha}/W_{\rm Br\gamma} = 10.5$ for $T = 10{,}000$ K and $n_e = 10^4$ cm^{-3}. Thus, the flux excess at 1.87 μm cannot be solely due to H I 3–4, even if we attribute all the flux at 2.166 μm to H I 4–7. As an aside, we argue that the 2.166 μm feature ($W \approx 5$ Å) is attributable to He II 8–14, noting that the ratio of flux in that line to flux in the 2.189 μm line (He II 7–10) is 1:4, identical to the ratio of recombination coefficients for the two associated transitions. Finally, it is likely that He II lines contribute most of the flux in the F187N bandpass. $W_{\rm He\,II\,7-10} = 20$ Å in the composite K-band spectrum. Consulting Hummer & Storey (1987) again, we find $W_{\rm He\,II\,5-6,1.8641\,\mu m}/W_{\rm He\,II\,7-10} = 9.6$, $W_{\rm He\,II\,6-8,1.8749\,\mu m}/W_{\rm He\,II\,7-10} = 2.5$, and $W_{\rm He\,II\,7-11,1.8762\,\mu m}/W_{\rm He\,II\,7-10} = 0.6$. The respective contributions to the flux in the F187N filter are $W_{\rm HeII5-6} = 190$ Å, $W_{\rm HeII6-8} = 50$ Å, and $W_{\rm HeII7-11} = 12$ Å. All totalled, we estimate, $W_{\rm HeII1.87\mu m} = 250$ Å, not too different from the measured values in Table 5. Note that the three He II lines do not all fall in the same part of the F187N filter; however, their line widths are broad enough to extend over most of the filter band pass in all three cases (see FMM99).

We conclude that both stars are likely $<$WC8, given the coincidence of the following facts: the above analysis indicates that the flux excess at 1.87 μm is mostly due to He II transitions, the composite K-band spectrum in FMM99 indicates very little hydrogen in either star, and the excess emission at 3.09 μm in the integrated light from both stars is ascribable to He II 8–11 (FMM99).

3.6.2. *Ionizing Flux*

Given the estimated ionizing flux from the various hot stars in the region, we can determine which stars are contributing to the ionization of the nebula. Lang et al. (1997) estimate that the nebula is ionized by $5.6(10^{48})$ H I ionizing photons s^{-1}. Assuming that the Pistol Star emits less than $4.4(10^{49})$ H I ionizing photons s^{-1} (see "H" model in F98) we find that it contributes less than 8% of the ionizing photons at the most intense location in the Pistol Nebula, assuming that the true distance between the hot stars and the nebula is $\sqrt{2}$ times the projected separation. An additional 85% of the ionizing flux can be produced by stars 235N and 235S (44%), 241 (18%), 151 (13%), and 240 (9%), where a first guess of the relative contributions are in parentheses. The remainder of the flux could come from other hot stars in the region (Figer et al. 1999). This distribution of ionizing flux is consistent with the fact that the nebular emission is most intense where the gas is closest to stars 235N, 235S, and 241. Note that if we use the "L" model in F98, then we would predict that the Pistol Star contributes an insignificant amount of ionizing flux compared to other nearby hot stars by the analysis above. In addition, the Pistol Star would produce 7 orders of magnitude fewer ionizing photons than what is required to ionize the nebula on its own.

4. DISCUSSION

In this section, we argue that the Pistol Nebula is the most massive LBV ejecta known and that the expanding gas in the nebula has been significantly slowed by the winds of nearby stars. We compare the nebula to other LBV nebulae and discuss the possibility that the ambient magnetic field might impact the shape of the nebula.

4.1. *The Pistol Nebula as LBV Ejecta*

We interpret the Pistol Nebula as expanding LBV ejecta in the presence of massive stars with dense winds and a strong ambient magnetic field. The classic identifying characteristics of luminous blue variable nebulae (LBVNs) include chemical enhancement relative to the local medium and a clear indication that gas is expanding from an LBV (Nota et al. 1995). Evidence for helium enhancement of the Pistol Nebula was given in Lang et al. (1997) and F98. If real, the enhancement is only slightly greater than solar, but this is consistent with the suggestion that the Pistol Star is in the early stages of an LBV phase (F98).

The dynamical evidence presented in this paper, coupled with the symmetry of the gas distribution with respect to the Pistol Star, both on the sky (Fig. 1) and in the position-velocity diagrams (Figs. 4*a*–4*d*), shows that gas in the nebula is expanding from the Pistol Star. We therefore suggest the following interpretation of the observed velocities. Gas in the Pistol Nebula was ejected with a velocity similar to the current terminal velocity of the stellar wind near the star, $v_{\rm wind} = 95$ km s^{-1} (F98). The current expansion velocity of the nebula, $v_{\rm expansion} = 60$ km s^{-1}, therefore indicates that the gas has been decelerated owing to interactions with the surrounding medium, a common occurrence for LBVNs (Nota et al. 1995). The far side of the expanding shell has been decelerated more than the near side, suggesting an interaction between the expanding shell and the winds from other cluster stars (see below). The above values of $v_{\rm wind}$ and $v_{\rm expansion}$ constrain the expansion timescale for the outer nebula to lie between 6000 and 9000 yr. The corresponding timescale for the inner shell is half that of the outer shell.

The mass of gas in the nebula is much higher than any other LBVN, $\approx 10\,M_\odot$. While this might suggest that much of the material has been swept up from the ambient local medium, such material would not be enhanced in helium. In addition, the enhanced helium content (and large nebular

mass) cannot be swept up material from the winds of the W-R stars in the cluster (see § 6.2 in F98). Instead of seeing the large nebular mass as a difficulty for the ejection hypothesis, it might be viewed as a natural consequence of the particularly large mass of the progenitor. Indeed, we might expect that more massive stars will produce more massive LBVN (Humphreys & Davidson 1994).

Could such a large mass be decelerated by the winds of the nearby WC stars? Equation (8) is satisfied if this is the case:

$$\rho_{\rm WC} v_{\rm WC}^2 = \rho_{\rm nebula}\, \delta\, \frac{\Delta V_{\rm expansion}}{\Delta t}, \qquad (8)$$

where $\rho_{\rm WC}$ is the average density of the winds from the WC stars at the location of the nebula, $\rho_{\rm nebula}$ is the density of gas in the expanding nebula, $v_{\rm WC}$ is the velocity of the winds, δ is the thickness of the expanding shell, $\Delta V_{\rm expansion}$ is the velocity change of the shell, and Δt is the time during which the velocity changed. We assume an average distance between the WC stars and the nebula of 0.6 pc, a total mass-loss rate in the WC star winds of $\approx 10^{-4}\ M_\odot\ {\rm yr}^{-1}$, and a wind velocity of 2000 km s^{-1}. The change in velocity for the redshifted gas is $95 - 10$ km s^{-1} $= 85$ km s^{-1}. Using values in § 3.4, we find $\Delta t \approx 6000$ yr, roughly equivalent to our estimate of the expansion time.

There is further evidence that the Pistol Nebula is circumstellar ejecta from the Pistol Star that is ionized by nearby hot stars. Moneti et al. (1999) present results of a spectroscopic study of the Pistol and of the cocoon stars in the Quintuplet Cluster. From ISOCAM CVF 5–17 μm spectroscopy, they find a nearly spherical shell of hot dust centered about the Pistol Star, clearly indicating that the shell is stellar ejecta. The continuum images show that the dust shell extends far to the south of the ionized portion of the nebula, consistent with the idea that the ionizing source is located outside the shell to the north. The ISO emission-line images confirm that most of the ionized material is along the northern border of the shell, and the morphology in these images is very similar to that of the H II region. The SWS spectrum of the nebula indicates a harder ionizing radiation than could be provided by the Pistol Star but that is consistent with ionization from Wolf-Rayet stars in the Quintuplet Cluster. Taken together, all these data are consistent with the idea that the Pistol Nebula is circumstellar ejecta mostly ionized by very hot stars in the core of the Quintuplet Cluster.

By most measures, the Pistol Nebula is typical, qualifying as a shell-type ejecta, such as AG Car, according to Nota et al. (1995). Even the northern knot, and the trail of emission between it and the star, are reminiscent of features in the "homunculus" of η Car (Currie et al. 1996). Table 6 lists characteristics of LBVNs, as adapted from Nota et al. (1995), with a new entry for the Pistol Nebula. Within errors, most of the values for the listed parameters are within in the range of values for other LBVNs, except for gas temperature and gas mass. The gas temperature is consistent with the relatively low temperatures for H II regions in the Galactic center (cf. Lang et al. 1997). So, the total nebular mass is the only truly extraordinary characteristic of the Pistol Nebula, being over a factor of 2 greater than the mass of the next most massive LBVN.

4.2. *Shaping of the Pistol Nebula by the Ambient Magnetic Field?*

The quasi-rectangular morphology of the nebula is not consistent with perfectly spherical expansion, although that is not unusual for the ejecta from LBVs (Nota et al. 1995), presumably because, in many cases, the ejections are themselves irregular and anisotropic. In the case of the Pistol Nebula, the ambient magnetic field in which the nebula is apparently embedded may have an important influence on the nebular geometry. Three considerations lead us to this conclusion.

First, the nebula is bounded by two nonthermal radio filaments (NTFs), which delineate the magnetic field direction (see Fig. 8). These filaments appear to be associated with the bundle of NTFs constituting the Radio Arc (Yusef-Zadeh & Morris 1987), and the uniformity of the filament orientation indicates that the magnetic field is perpendicular to the Galactic plane throughout this region (indeed, Morris 1994 [see also Chandran, Cowley, & Morris 1999] has argued that the magnetic field is perpendicular to the Galactic plane throughout the central 100–150 pc).

TABLE 6

LBV Nebulae[a]

Star (1)	$\log(L/L_\odot)$ (2)	$V_{\rm wind}$ (km s^{-1}) (3)	Nebular Size (pc) (4)	$v_{\rm gas}$ (km s^{-1}) (5)	Dynamical Time (10^4 yr) (6)	$M_{\rm gas}$ ($M_\odot$) (7)	$M_{\rm dust}$ ($M_\odot$) (8)	N_e (cm^{-3}) (9)	T_e (K) (10)
Pistol Star.....	6.6	95	0.8 × 1.2	60	0.6–0.9	11	0.003	1200	3600[b]
AG Car.....	6.2	80–250	1.1 × 1.0	70	0.84	4.2	0.013	800	9000
R127	6.0	~150	1.9 × 2.2	28	4.0	3.1	...	1000	...
η Car	6.5[c]	...	0.2	600	0.015	...	0.01	...	...
He 3-519	4.8	365	2.28	61	1.8	2.0	0.0066	300	8000
S119	...	...	1.9 × 2.1	25	5.0	1.7	...	800	...
WRA 751	5.8	...	0.8	20–60	...	...	...	...	...
HD 168625.....	5.4	250	0.06	20	0.3	0.03	0.0003	630	...
HR Car.....	5.7	145–170	0.98	50	1.0	2.1	0.0010	600	<12,500
R143	6.0	...	3.5	...	...	...	...	...	...
P Cyg.....	5.2	206	0.2	140	0.01–0.01	0.0092	...	1000	5000

Notes.—Col. (1): Star name. Col. (2): Luminosity. Col. (3): Velocity of the stellar wind. Col. (4): Size of the nebula. Col. (5): Gas expansion velocity. Col. (6): Age of the nebula. Col. (7): Ionized gas mass. Col. (8): Dust mass. Col. (9): Electron density. Col. (10): Electron temperature.

[a] All values are from Table 1 in Nota et al. 1995 and references therein, unless noted otherwise.

[b] From Lang et al. 1997.

[c] η Car is probably multiple (Damineli, Conti, & Lopes 1997).

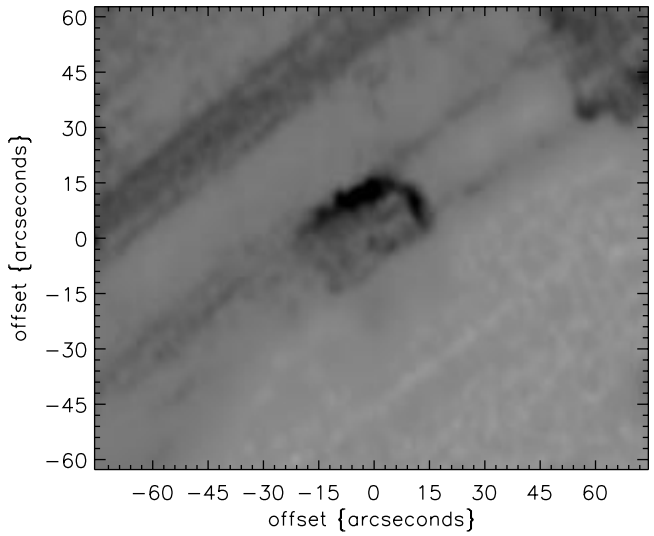

FIG. 8.—Log gray-scale plot of 6 cm radiograph. The origin is set at the location of the Pistol Star. The nonthermal filaments can clearly be seen, bounding the Pistol Nebula on its northeast and southwest sides.

The second reason to suspect the importance of the magnetic field for shaping the geometry of the nebula is the elongation and orientation of the nebula: it is elongated along the magnetic field, as would be expected if the ambient field were strong enough to constrain the expansion in the direction perpendicular to the field. On the other hand, the Pistol Nebula has a roughly rectangular morphology, with the long sides parallel to the field, as defined by the bounding NTFs, while the shape to be expected for expansion of a spherical piston into a strong magnetic field has been predicted to be more oval, at least in the earlier stages of the expansion (Insertis & Rees 1991; Ferriere, Mac Low, & Zweibel 1991). In any case, the minor axis dimension and the axial ratio of the nebula should be consistent with the ambient magnetic field strength, if indeed the field is responsible for shaping the nebula. Noting the apparent rigidity of the nonthermal filaments, especially where they interact with molecular clouds or H II regions, Yusef-Zadeh & Morris (1987, see also Morris 1994) have argued that the field strength within the filaments, and perhaps throughout the Galactic center region, is at least 1 mG.

To illustrate that such a strong field can have an important dynamical effect on the ejecta from the Pistol Star, we equate the ram pressure of the expanding wind, ρV_w^2, with the magnetic pressure, $B^2/8\pi$, in order to estimate the stagnation radius, r_m, in the direction perpendicular to the magnetic field. With $\rho = \dot{M}/4\pi r_m^2 V_w$, where $\dot{M}$ is the mean mass loss rate during an ejection event, we obtain

$$r_m = 0.12 \text{ pc} \left(\frac{\dot{M}}{10^{-4}\ M_\odot\ \text{yr}^{-1}}\right)^{1/2} \times \left(\frac{V_{\text{expansion}}}{100\ \text{km s}^{-1}}\right)^{1/2} \left(\frac{1\ \text{mG}}{B}\right). \quad (9)$$

The semiminor axis of the nebula is about 10″, or 0.39 pc at the distance to the Galactic center. This distance can be made to agree with the calculated stagnation radius if (1) the initial ejection velocity was substantially higher than the current expansion velocity or (2) the mass ejection rate during an outburst substantially exceeds $10^{-4}\ M_\odot\ \text{yr}^{-1}$ and/or the B field is weaker than 1 mG.

Either of these possibilities is plausible, given the values in Table 6; however, it is difficult to see how the strength of the magnetic field can be significantly below 1 mG (Yusef-Zadeh & Morris 1987). It seems likely that the mass-loss rate during an eruption is substantially enhanced over the time-averaged value. Assuming, for example, that $r_{\text{outer}} = 0.60$ pc, $r_{\text{inner}} = 0.50$ pc, $v_{\text{eruption}} = 95$ km s^{-1}, and $M_{\text{eruption}} = 11\ M_\odot$, we find $\dot{M} = 0.02\ M_\odot\ \text{yr}^{-1}$, giving $r_m = 1.7$ pc. This value of r_m, and that derived from an assumed constant mass-loss rate, bracket the observed value; given the uncertainties in the various parameters, we regard the observed minor axis size of the Pistol Nebula to be consistent with the possibility that it has been magnetically shaped.

The third consideration is the brightness discontinuity of the bounding filaments across the boundary of the nebula. The brightness of each of the bounding filaments changes along their lengths from one side of the nebula to the other by a factor of ≈ 2, indicating that their emissivity has undergone a discontinuity somewhere along the boundary. In addition, the northern filament becomes two filaments on the eastern side of the nebula. This not only supports the notion that the bounding NTFs are interacting with the nebula, but it may point to the nebular boundary as a source or a sink for relativistic electrons. In their model for the principal NTFs of the Radio Arc, Serabyn & Morris (1994) hypothesized that the H II region G0.18−0.04 is the source of relativistic electrons for those filaments because of the pronounced brightness discontinuities they suffer where they encounter that H II region. The acceleration mechanism in this model is magnetic field line reconnection at the interface between the H II region and the ambient interstellar medium. A related model can be applied to G0.15−0.05, except that in this case, there is no molecular cloud underlying the H II region. The model of Rosner & Bodo (1996) seems particularly apt because it is based upon a stellar wind from a hot star. These authors suggest that the electron acceleration takes place at the wind's termination shock. However, they consider winds with velocities ~ 1000 km s^{-1}, or more than an order of magnitude larger than that of the Pistol Star, so their results will have to be scaled accordingly.

5. CONCLUSIONS

Our new imaging and spectroscopic data suggest that the Pistol Star has recently ($\lesssim 10^4$ yr) ejected a massive circumstellar nebula, distributed in two shells centered on the Pistol Star, which is being photoionized by nearby hot stars in the Quintuplet Cluster. The ejected mass is $\approx 10\ M_\odot$, over a factor of 2 times the most massive ejecta from an LBV. The nebula has been ejected in the presence of a strong magnetic field and powerful winds of nearby hot stars, offering an opportunity to test wind-wind interaction models and models of magnetically confined outflows.

We gratefully acknowledge the late Chris Skinner of STScI for providing assistance in performing the *HST* observations. We thank Christine Ritchie of STScI for calibrating the data. We thank Zolt Levay of STScI for producing the color composite image in Figure 1. We thank L. E. Bergeron of STScI for "cleaning" the images of bad pixels using his "imclean" IDL script. We thank Antonella Nota for providing the original LaTex code for Table 6. We thank Tony Marston for discussions concerning the impact

of massive stars on their local medium. We thank Andrea Moneti for useful discussions concerning his ISO results on the Pistol Star. We also thank Rodger Thompson, Marcia Rieke, and the NICMOS team for providing assistance in reducing our data. Support for this work was provided by NASA through grant GO-07364.01-96A from the Space Telescope Science Institute, which is operated by AURA, Inc., under NASA contract NAS5-26555. The CGS4 spectra were obtained as part of the UKIRT Service Programme. UKIRT is operated by the Joint Astronomy Centre on behalf of the United Kingdom Particle Physics and Astronomy Research Council.

REFERENCES

Chandran, B., Cowley, S. & Morris, M. 1999, ApJ, submitted
Conti, P. S. 1984, in IAU Symp. 105, Observational Tests of Stellar Evolution Theory, ed. A. Maeder & A. Renzini (Dordrecht: Reidel), 233
Cotera, A. S., Erickson, E. F., Allen, D. A., Simpson, J. P., Colgan, S. W. J., & Burton, M. G. 1994, in Nuclei of Normal Galaxies: Lessons Learned from the Galactic Center, ed. R. Genzel & A. I. Harris (Dordrecht: Kluwer), 217
Cotera, A. S., Erickson, E. F., Colgan, S. W. J., Simpson, J. P., Allen, D. A., & Burton, M. G. 1996, ApJ, 461, 750
Currie, D. G., et al. 1996, AJ, 112, 1115
Damineli, A., Conti, P. S., & Lopes, D. F. 1997, NewA, 2, 107
Ferriere, K. M., Mac Low, M.-M., & Zweibel, E. G. 1991, ApJ, 375, 239
Figer, D. F. 1995, Ph.D. thesis, Univ. of California, Los Angeles
Figer, D. F., McLean, I. S., & Morris, M. 1995, ApJ, 447, L29 (FMM95)
———. 1999, ApJ, 514, 202 (FMM99)
Figer, D. F., McLean, I. S., & Najarro, F. 1997, ApJ, 486, 420
Figer, D. F., Najarro, F., Morris, M., McLean, I. S., Geballe, T. R., Ghez, A. M., & Langer, N. 1998, ApJ, 506, 384 (F98)
Glass, I. S., Matsumoto, S., Carter, B. S., & Sekiguchi, K. 1999, MNRAS, in press
Harris, A. I., Krenz, T., Genzel, R., Krabbe, A., Lutz, D., Poglitsch, A., Townes, C. H., & Geballe, T. R. 1994, in Nuclei of Normal Galaxies: Lessons Learned from the Galactic Center, ed. R. Genzel & A. I. Harris (Dordrecht: Kluwer), 223
Hummer, D. G., & Story, P. J. 1987, MNRAS, 224, 801
Humphreys, R. M., & Davidson, K. 1994, PASP, 106, 1025
Insertis, F. M., & Rees, M. J. 1991, MNRAS, 252, 82
Lang, C. C., Figer, D. F., Goss, M., & Morris, M. 1999, AJ, in press
Lang, C. C., Goss, W. M., & Wood, D. O. S. 1997, ApJ, 474, 275
Marston, A. P., & Dickens, R. J. 1988, A&A, 193, 27
Moneti, A., Blommaert, J. A. D. L., Najarro, F., Figer, D. F., & Stolovy, S. 1999, in Proc. of The Universe as Seen by *ISO*, ed. P. Cox & M. F. Kessler (ESA SP-427; Noordwijk: ESA), 723
Moneti, A., Glass, I. S., & Moorwood, A. F. M. 1994, MNRAS, 268, 194
Morris, M. 1994, in The Nuclei of Normal Galaxies: Lessons from the Galactic Center, ed. R. Genzel & A. I. Harris (NATO ASI Ser. C, 445; Dordrecht: Kluwer), 185
Nagata, T., Hyland, A. R., Straw, S. M., Sato, S., & Kawara, K. 1993, ApJ, 406, 501
Nota, A., Livio, M., Clampin, M., & Schulte-Ladbeck, R. 1995, ApJ, 448, 788
Piña, R. K., & Puetter, R. C. 1993, PASP, 105, 630
Puetter, R. C. 1995, Int. J. Image Sys. Tech., 6, 314
Puetter, R. C., & Yahil, A. 1999, in ASP Conf. Ser. 172, Astronomical Data Analysis Software and Systems VIII, ed. D. Mehringer, R. Plante, & D. Roberts (San Francisco: ASP), in press
Reid, M. J. 1993, ARA&A, 31, 345
Rieke, G. H., Rieke, M. J., & Paul, A. E. 1989, ApJ, 336, 752
Rosner, R., & Bodo, G. 1996, ApJ, 470, L49
Schneider, S. E., Terzian, Y., Purgathofer, A., & Perinotto, M. 1983, ApJS, 52, 399
Serabyn, E., & Güsten, R. 1991, A&A, 242, 346
Serabyn, E., & Morris, M. 1994, ApJ, 424, L91
Simpson, J. P., Colgan, S. W. J., Cotera, A. S., Erickson, E. F., Haas, M. R., Morris, M., & Rubin, R. H. 1997, ApJ, 487, 689
Timmermann, R., Genzel, R., Poglitsch, A., Lutz, D., Madden S. C., & Nikola, T. 1996, ApJ, 466, 242
Wynn-Williams, C. G., Becklin, E. E., Matthews, K., & Neugebauer, G. 1978, MNRAS, 183, 237
Yusef-Zadeh, F., & Morris, M. 1987, AJ, 94, 1178
Yusef-Zadeh, F., Morris, M., & van Gorkom, J. H. 1989, in IAU Symp. 136, The Center of the Galaxy, ed. M. Morris (Dordrecht: Kluwer), 275